gouttelettes d'eau sur une pastille de Nickel chauffée par induction électromagnétique. La température face-arrière de l'échantillon de nickel est mesurée à l'aide d'une caméra infrarouge, et le flux extrait à la paroi est estimé par un modèle d'inversion semi-analytique tenant compte de la conduction dans la pastille ainsi que des pertes convective et radiative. En parallèle, l'échauffement des gouttes est caractérisé à l'aide de la fluorescence induite par laser à deux couleurs. Cette technique a été récemment étendue à de l'imagerie dans le cadre de cette étude. Elle permet d'estimer la chaleur sensible gagnée par les gouttes lors de l'impact. La paroi est maintenue à une température supérieure à la température de Leidenfrost, tandis que le nombre de Weber des gouttes incidentes est modifié de manière à obtenir des rebonds et des éclatements. La comparaison entre la chaleur sensible gagnée par les gouttes et le flux extrait à la paroi permet finalement d'évaluer le flux de chaleur prélevée par évaporation. Les contributions au refroidissement de ces flux varient de manière significative en fonction du diamètre des gouttes, mais aussi du nombre de Weber des gouttes incidentes.

Nomenclature

a	diffusivity [m^2/s]
c	dye concentration [mol/L]
Cp	heat capacity [$kJ\,kg^{-1}K^{-1}$]
D	droplet diameter [m]
f	injection frequency [hz]
I_0	laser intensity [W]
K	Mundo number
L_v	latent heat [kJ/kg]
m	droplet mass [kg]
Oh	Ohnesorge number
p	Laplace parameter
Q_l	sensible heat gained by the liquid [J]
R_0	reference ratio
R_f	fluorescence ratio
T	temperature [K]
V	measurement volume
V_d	droplet velocity [m/s]
V_n	normal droplet velocity [m/s]
W	transmittance
We	Weber number
Z	impedance [$K\,m\,W^{-1}$]

Symbols

α	droplet incidence angle [°] or eigenvalues
γ	surface tension [N m]
δ	Dirac distribution or Kronecker symbol
ε	cooling efficiency
λ	wavelength [nm] or thermal conductivity [$W\,m^{-1}\,K^{-1}$]
μ	dynamic viscosity [Pa s]
ρ	density [kg/m^3]
Φ_w	heat removed from the wall by a single droplet [J]
Φ_{vap}	heat taken by the evaporation [J]

Subscripts

inj	initial condition at the injection
l	liquid phase
m	averaged in the droplet
obs	observed
v	vapor
w	wall

Superscripts

F, R	front, rear face
EQ	equivalent
$\bar{}$	Laplace transform
$\tilde{}$	Hankel transform

1. Introduction

In aero-engines, droplet/wall interaction phenomena have a considerable influence on the mixture formation process and on wall heat fluxes. Impinging droplets may rebound, splash into secondary droplets or form a liquid film onto the solid surface [1]. Droplet rebound and splashing is also a mechanism for the back penetration of the fuel vapor in the central region of the combustion chamber where the gas temperature is high enough for ignition. Droplet/wall interactions can also be found in cooling applications, which require a high heat dissipation rate. Spray quenching is very efficient compared to other cooling techniques. The main reason is that vapor can easily escape even if the temperature of the wall is well above the Leidenfrost temperature. However an optimization of these applications needs a complete understanding of the complex fluid flow and heat transfer characteristics when sprays interact with hot surfaces. The modeling of each physical phenomenon occurring in the combustion chamber is required to improve the accuracy of existing numerical codes. Due to the complexity of a dense spray, elementary phenomena are studied as basic experiments using monosized jets (droplets having all the same size and velocity and being regularly spaced).

The impingement of droplets on solid surfaces has received a considerable attention throughout the decades. Many studies have been focused on the impact conditions that can occur at high or low droplet velocity, with deep or shallow

liquid film, on hot or cold solid surfaces. Depending on these conditions, different behaviors can occur: the drops can spread over the solid surface, they can splash by creating a crown and droplet rebounds are also possible particularly on hot surfaces above the Leidenfrost temperature. Extensive experimental investigations were carried out to determine the parameters influencing the behavior of a single drop impact in order to characterize their respective influence. Some of these parameters describe the geometry and the dynamic of the drops [2,3], some refer to the physical properties of the liquid [2,4] or the solid surface [5]. Correlations based on dimensionless numbers characterizing the relative magnitude of the forces acting on the impinging droplet and estimated with the physical properties of the liquid before impact, i.e. Reynolds, Weber and Ohnesorge numbers [6] have been found.

This study concerns the non wetting conditions observed when the wall temperature is above the Leidenfrost temperature, which corresponds to the film boiling regime. A thin vapor layer forms quasi-instantaneously between the droplet and the wall and prevents the droplet to wet the wall. The splashing and the rebound of the droplet are the only behavior that can occur, depending on the size of the droplet and its normal component of velocity. An increase of the Weber number promotes the splashing [1]. We have firstly focused on the film boiling regime where the vapor cushion formed between the droplet and the solid insulates the droplet from the hot sample and thus limits drastically the heat transfer [7].

Heat transfers were generally characterized using thermocouples embedded in the sample thickness. It has been possible to monitor the history of the surface temperature at the location of the droplet impingement [8]. The heat flux to the wall was also estimated when the experimental set-up was designed to ensure a one-dimensional heat flux along the instrumented section containing a set of thermocouples. Advanced methods are even less intrusive and involve infrared thermography. Nevertheless, if measurements related to the wall provide valuable data to quantify the efficiency of the cooling, they have only a limited interest when focusing on the heat transfer occurring within the liquid phase. In particular, questions remain concerning the respective level of the droplet sensible heat variation and the heat lost due to liquid vaporization. To address this issue, it is necessary to use different measurement techniques. An inherent difficulty is the estimation of the mass of liquid evaporated during the droplet/wall interaction. To the best of our knowledge, few experimental data can be found in the literature for the mass loss during the impact in the splashing regime. In the bouncing regime, the ratio between outgoing and impinging liquid mass was evaluated by Le Clercq [9], using phase doppler measurements (PDA) and digital image processing. Although a correlation is provided by Le Clercq [9] and Rosa et al. [10] based on these measurement data, the accuracy of these direct measurements is questionable. The outcoming droplets are strongly deformed after their impingement and an accurate measurement of their volume or their mass is a real challenge with any optical method. According to [9] and [10], the variation in mass due to evaporation is rather important, about 25% for most of the rebound. This largely overestimates the experimental values by Watchers and Westerling [11] that were obtained using a completely different approach. Watchers and Westerling [11] collected the vapor expelled by the droplets and measured the mass of this vapor after condensation. The vapor was found to represent generally between 2 and 5% percent of the initial liquid mass.

Presently, a quite different strategy has been undertaken. The evaporation (i.e. the change in droplet size) is not directly measured but it is estimated indirectly from the application of energy conservation. All the heat fluxes involved in the cooling (namely the sensible heating of the liquid and the heat extracted from the wall) are measured except the heat flux associated with evaporation.

This article is an experimental study involving several measurement techniques for characterizing the heat transfer within the liquid phase and at the wall to be cooled. The temperature variation of the droplet is measured using a new optical technique: the two-color laser induced fluorescence (2cLIF) thermometry. In addition, an infrared camera measures the temperature field in the rear face of a thin nickel plate. A semi-analytical inverse heat conduction model allows estimating the heat flux on the front face of the plate where the droplets impinge. Finally, the heat flux lost by the wall and due to droplet/wall interaction is compared to the sensible heat stored in the outgoing droplets. This allows estimating the heat flux associated with evaporation of the drops.

2. Droplet generation and experimental set-up

In order to study droplet/wall interactions, an experimental set-up was specifically designed. A sketch of the experimental set-up is shown in Fig. 1. A linear monodisperse droplet stream is generated by the disintegration of a cylindrical liquid jet. The breakup is driven by a Rayleigh-type instability that can be triggered by mechanical vibrations using a piezoceramic. For some specific frequencies of the vibrations, the liquid jet split into equally spaced and monosized droplets. The size of the injector orifice and the inlet pressure can be changed from an experiment to another, which allows to some extents adjusting separately the diameter D_d, the frequency f and the velocity V of the droplets. In this study, the droplets range from 80 μm to 250 μm while their velocity is of the order of a few m/s. The droplet generator can be rotated precisely to any prescribed angle α of incidence. The temperature of the injector body is regulated while the liquid temperature is measured by a thermocouple placed just before the outlet of the injector. Water droplets impact periodically a thin disk of nickel (thickness is 500 μm and radius $R = 12.5$ mm) which is heated using an electromagnetic inductor device. In this contactless heating technique, the distribution of the heat sources in the skin depth of the metallic sample is perfectly controlled. The low thickness of the nickel disc allows limiting the damping of the thermal response at the rear face (side of the sample opposite to the droplet impact). The upper surface of the nickel on which the droplets are impacting, is polished so as to obtain a very smooth surface. The oxidation of nickel occurs easily when the wall temperature exceeds 500 °C.

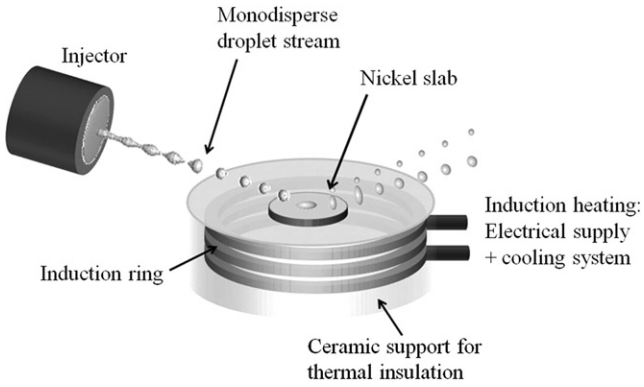

Fig. 1. Experimental set-up.

An oxide layer covers the surface of the nickel disk. This green and gray layer of nickel oxide that covers the disc is very stable, and did not provide a significant change of the overall roughness. In addition, the oxidation increases the radiative emissivity of the wall.

3. Shadowgraphy for measuring droplets size and velocity

A high-speed (HS) camera is used to visualize the shape of the droplet stream impinging onto the heated wall. The HS camera is a Phantom v710 equipped with a 12-bits CMOS sensor that can provide up to 7500 fps at full resolution (1280 × 800 pixels). It is used with a reduced resolution to perform the image acquisition at a much higher frame rate, typically in the order of 100,000 fps. This is sufficient to resolve in time the droplet/wall interactions in the experimental conditions encountered in this study. The droplets are illuminated from behind using a very bright light source (a 400 W HMI lamp with a parabolic reflector). A zoom lens allows observing in detail the droplet deformation and possible splashing, with a field of view ranging from 400 μm to 3 mm. The images are then processed with a homemade detection and tracking program in order to determine the main features of the impact. A genetic algorithm is used for the tracking of the particle trajectories. It is based on the multi-hypothesis tracking method proposed by Reid [12]. Boulesteix [13] describes an adaption of this method for the tracking of droplets. Joint distributions of the droplets size and velocity can be derived from the processing of the images. Other important parameters such as the incident angle, the normal and tangential velocities, the residence time, or the spreading diameter of the droplets can be also determined.

4. Two-color laser induced fluorescence for measuring the droplet temperature

Different optical techniques have been developed in the past decades to characterize the droplet temperature. However, for some methods like the rainbow refractometry, a perfect spherical shape of the droplet is required to obtain a correct temperature after inversion. The two-color laser induced fluorescence (2cLIF) has already demonstrated its ability to characterize the temperature of droplets in various situations including droplet evaporation in either inert or reactive flows [14,15]. The technique was also used to determine the droplet change in temperature during their impingement onto a heated solid surface [16]. In this study, the 2cLIF thermometry was restricted to point-wise measurements, which imply a cumbersome point-by-point scanning to reconstruct the temperature distribution in the liquid phase of the flow. More recently, the technique was extended to planar laser induced fluorescence (PLIF) in order to obtain the temperature field [17].

The 2cLIF thermometry is based on the measurement of the fluorescence intensity of a single dye tracer. In liquids, the fluorescence quantum yield is strongly influenced by the quenching, which depends on the temperature. When a laser beam induced the fluorescence of a dye dissolved into a liquid medium, the fluorescence signal I emerging from the medium toward the detector can be expressed as:

$$I_f(\lambda) = K_{opt}(\lambda) K_{spec}(\lambda) I_0 c V \exp\left(\frac{\beta(\lambda)}{T}\right) \tag{1}$$

where K_{opt} is a parameter depending on the optical properties of the detection system (e.g. the solid angle of the detection, the spectral sensitivity of the detectors), K_{spec} is a parameter depending on the spectroscopic properties of the tracer in its solvent. c is the concentration in dye molecules and the product c. V corresponds to the number of molecules that are illuminated by the laser beam while in the field of view of the detector. I_0 is the intensity of the laser beam before crossing the absorbing medium. In Eq. (1), it is implicitly assumed that the absorption of the laser beam and the fluorescence can be neglected along the ray path in the liquid medium. Fig. 2 shows the evolution of the fluorescence emission spectrum of Rhodamine 640 (Rh640, $C_{32}H_{31}N_2O_3{\cdot}ClO_4$, also called rhodamine 101) that has been selected for this study. A decrease in the fluorescence intensity is clearly observed when increasing the temperature. The evolution of $\beta(\lambda)$ is also superimposed

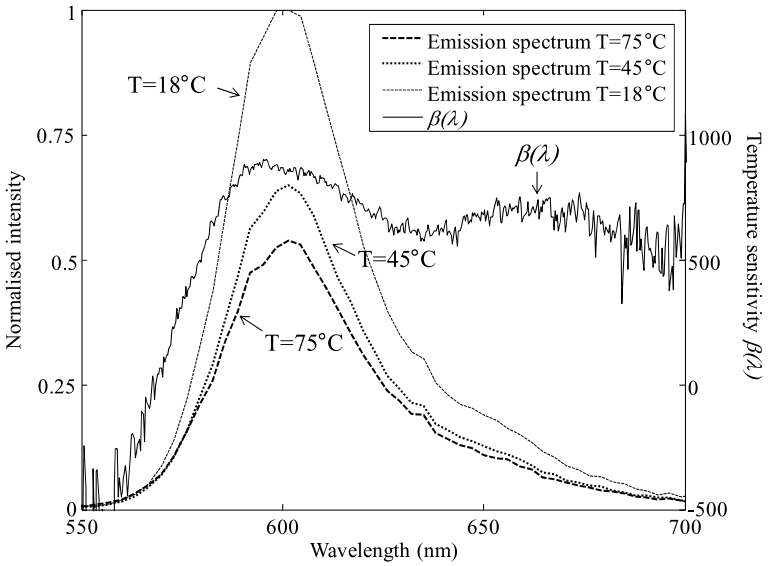

Fig. 2. Fluorescence spectrum of Rh640 dissolved in water and the wavelength dependence of $\beta(\lambda)$.

in the figure. The value $\beta(\lambda)$ varies significantly between the right and the left sides of the spectrum, meaning that the effect of temperature is not the same for all the wavelengths in the fluorescence spectrum. Optical filters are used in the measurement to select specific spectral bands of the fluorescence emission. For a given spectral band i, the fluorescence intensity $I_f(\lambda)$ is integrated over the wavelength range $[\lambda_{i,1}, \lambda_{i,2}]$. Based on experimental measurements, Lavieille et al. [18] suggest approximating this expression as:

$$I_{f,i} = \int_{\lambda_{i,1}}^{\lambda_{i,2}} I(\lambda)\,\mathrm{d}\lambda \approx K_{opt,i} K_{spec,i} I_I c V \exp\left(\frac{A_i}{T^2} + \frac{B_i}{T} + C_i\right) \tag{2}$$

In this expression, A_i and B_i are specific to a given combination of dye, solvent, excitation wavelength, and spectral band. In contrast, C_i depends on the exact configuration of the experimental system and can change from one measurement configuration to another. The ratio R_f of the intensities of two different spectral bands is given by:

$$R_f = \frac{I_{f,1}}{I_{f,2}} = \frac{K_{opt,1} K_{spec,1}}{K_{opt,2} K_{spec,2}} \exp\left(\frac{A}{T^2} + \frac{B}{T} + C\right) \tag{3}$$

where $X = X_1 - X_2$ stands for $X = A$, B or C. The ratio of the fluorescence intensity of two bands allows eliminating the effects of parameters that are unknown or difficult to control such as the variations in laser intensity, the tracer concentration or the measurement volume during the acquisitions. When the technique is applied in imagery, only A and B do not depend on the pixel position in the image. All other variables can change from one pixel to the other, especially the parameters $K_{opt,i}$, $K_{spec,i}$ and C. Even under isothermal conditions, the fluorescence ratio is not necessarily uniform. To eliminate the influence of the detection system, a reference measurement at a known temperature T_0 (with the same optical configuration as for the measurement) is recorded. Denoting R_0 the fluorescence ratio obtained in the reference measurement, the temperature can be derived from:

$$\ln\left(\frac{R_f}{R_0}\right) = A\left(\frac{1}{T^2} - \frac{1}{T_0^2}\right) + B\left(\frac{1}{T} - \frac{1}{T_0}\right) \tag{4}$$

Once A and B are known, Eq. (4) can be used to determine the liquid temperature. These parameters are obtained by a calibration in a temperature-controlled cell using the full measurement system in particular for the selected spectral bands of detection. These bands correspond to the ranges [555–565 nm] and [635–685 nm] and are selected with regards to their intensity level as well as their sensitivity to the temperature (Fig. 2). The variation of the fluorescence of ratio is about 1.4%/K which seems in practice enough to measure the droplet temperature with an accuracy of about 2 °C.

The measurement system of the 2cPLIF technique is illustrated in Fig. 3. The excitation of Rh640 is achieved by means of a CW Nd:YAG laser (Laser Quantum Finesse, 6 W@532 nm). An arrangement of spherical and cylindrical lenses provides a laser sheet with a thickness of 220 μm and a height of 16 mm in the measurement zone. This latter is observed by a Questar QM-1 long distance microscope, which is positioned at right angle at a working distance of about 84 cm. The microscope field of view is then about 3.5×3.5 mm^2. A holographic filter (Notch Plus, Kayser Optical) is used to block the